ARMY RESEARCH LABORATORY

Progress in the Development of a Multiphase Turbulent Model of the Gas/Particle Flow in a Small-Caliber Ammunition Primer

by John R. Schmidt and Michael J. Nusca

ARL-TR-3860 **August 2006**

NOTICES

Disclaimers

The findings in this report are not to be construed as an official Department of the Army position unless so designated by other authorized documents.

Citation of manufacturer's or trade names does not constitute an official endorsement or approval of the use thereof.

Destroy this report when it is no longer needed. Do not return it to the originator.

Army Research Laboratory
Aberdeen Proving Ground, MD 21005-5066

ARL-TR-3860 **August 2006**

Progress in the Development of a Multiphase Turbulent Model of the Gas/Particle Flow in a Small-Caliber Ammunition Primer

John R. Schmidt and Michael J. Nusca
Weapons and Materials Research Directorate, ARL

REPORT DOCUMENTATION PAGE

Form Approved
OMB No. 0704-0188

1. REPORT DATE *(DD-MM-YYYY)*	2. REPORT TYPE	3. DATES COVERED (From - To)
August 2006	Final	January 2005–December 2005

4. TITLE AND SUBTITLE
Progress in the Development of a Multiphase Turbulent Model of the Gas/Particle Flow in a Small-Caliber Ammunition Primer

5a. CONTRACT NUMBER
DAAD1703C0070

5b. GRANT NUMBER

5c. PROGRAM ELEMENT NUMBER

6. AUTHOR(S)
John R. Schmidt and Michael J. Nusca

5d. PROJECT NUMBER
622618H8000

5e. TASK NUMBER

5f. WORK UNIT NUMBER

7. PERFORMING ORGANIZATION NAME(S) AND ADDRESS(ES)
U.S. Army Research Laboratory
ATTN: AMSRD-ARL-WM-BD
Aberdeen Proving Ground, MD 21005-5066

8. PERFORMING ORGANIZATION REPORT NUMBER
ARL-TR-3860

9. SPONSORING/MONITORING AGENCY NAME(S) AND ADDRESS(ES)

10. SPONSOR/MONITOR'S ACRONYM(S)

11. SPONSOR/MONITOR'S REPORT NUMBER(S)

12. DISTRIBUTION/AVAILABILITY STATEMENT
Approved for public release; distribution is unlimited.

13. SUPPLEMENTARY NOTES

14. ABSTRACT
There is significant experimental evidence that burning particles of various chemical compositions and sizes are ejected from gun primers and that these particles interact with the propellant grains during main charge ignition. This explicit ignition phenomenon is thought to be incompatible with the implicit treatment of primer function in conventional interior ballistics codes and models. Generally, the primer efflux is treated as a hot gas that evolves from a specified region in the model's representation of the gun chamber (usually along the chamber centerline and near the breech). What amounts to an igniter table is arrived at by experimental means and by careful calibration of the interior ballistics simulation using gun firing data. With the advent of multidimensional, multiphase interior ballistics codes which employ coupled Eulerian-Lagrangian schemes to explicitly treat both the gas and solid phase, the time is ripe for a primer model that is commensurate with the availability of such an interior ballistics model. Progress in the development of a primer model that is compatible with the ARL-NGEN3 interior ballistics code and small-caliber weapons is described herein. The model is based on the One Dimensional Turbulence modeling approach that has recently emerged as a powerful tool in multiphase simulations. Initial results are shown for the model run as a stand-alone code and are compared to recent experiments with small-caliber primers.

15. SUBJECT TERMS
interior ballistics, turbulence, primer, CFD, two-phase flow

16. SECURITY CLASSIFICATION OF:			17. LIMITATION OF ABSTRACT	18. NUMBER OF PAGES	19a. NAME OF RESPONSIBLE PERSON
a. REPORT	b. ABSTRACT	c. THIS PAGE			John R. Schmidt
UNCLASSIFIED	UNCLASSIFIED	UNCLASSIFIED	UL	44	19b. TELEPHONE NUMBER (*Include area code*) 410-278-5510

Standard Form 298 (Rev. 8/98)
Prescribed by ANSI Std. Z39.18

Contents

List of Figures

List of Tables

Acknowledgments

The first author would like to thank Dr. Alan R. Kerstein, the inventor of One Dimensional Turbulence, for his continued help. The authors would also like to thank the following: Dr. Anthony Kotlar for his help and expertise with Nasa-Glenn thermodynamics code, Mr. Anthony Williams for keeping us apprised of the ongoing experiments, and Dr. Pamela Kaste for discussions on the analytical work on the primers. The Program Manager – Maneuver Ammunition Systems is acknowledged for continued support of this effort. This research was performed while the first author held a National Research Council Research Associateship at the U.S. Army Research Laboratory.

INTENTIONALLY LEFT BLANK.

1. Introduction

Numerical simulation of the interior ballistics (IB) of large-caliber guns has steadily progressed over the last few decades. As a testament to this progress, the U.S. Army Research Laboratory (known prior to 1992 as the Ballistics Research Laboratory) has played a major role in the development and popularization of a number of IB codes such as IBHVG2 (*1*), NOVA (also known as XKTC) (*2*, *3*), and NGEN (*4*–*6*), which progress in both model complexity and dimensionality (i.e., 0-D, 1-D, and 2-D/3-D, respectively). A good review of the utility of this suite of IB codes is given by Horst and Nusca (*7*). Through this ambitious and successful progression of IB code development, one area of research that has been paid less attention is the fidelity with which the ignition system (i.e., the primer in small-caliber guns, the primer and flashtube in medium-caliber guns, and the primer and igniter-tube in large-caliber guns) is represented. One notable exception is an igniter sub-model implemented in the NOVA code for a 105-mm tank gun charge of low-vulnerability gun propellant (*8*, *9*). In this model, the primer efflux was treated as gaseous with an added condensing phase. This phase was to mimic some effects of a true solid phase which would represent the particles that are a major part of most primer efflux and will be addressed in this report.

There is significant evidence that burning particles of various chemical compositions and sizes are ejected from gun primers (*10*–*12*) and interact with the propellant grains during charge ignition. Numerical investigation of this ignition phenomena was previously intractable using the NGEN code because the code utilizes an explicit, particle-based treatment of the propellant but not the igniter material. It would then follow that such an IB code could be upgraded to model the interaction of the discrete primer particles and the discrete propellant particles simultaneously. With the advent of the ARL-NGEN3 IB code, which employs a coupled Eulerian-Lagrangian scheme to explicitly treat both the continuous (gases) and discrete (solid) phases, the time is ripe for a primer model that is commensurate with the availability of such an IB model. Progress in the development of a primer model that is compatible with the ARL-NGEN3 IB code is the subject of this report.

The conventional ignition system for a large-caliber (120 mm, figure 1) gun consists of a long, narrow metallic tube that is mounted on the gun chamber breech and extends into the gun chamber along the centerline (*11*). The tube is perforated along its length, which allows venting (primarily in the radial direction) of igniter gases from burning igniter material loaded within. This energetic material generally consists of either long sticks of Benite or tightly-packed particles (black powder) designed to rapidly ignite and flamespread producing hot gases and hot solid particles. The efflux from the primer tube is used to ignite the solid propellant gun charge. Conventional modeling of this igniter tube generally consists of a tabular input of gaseous mass

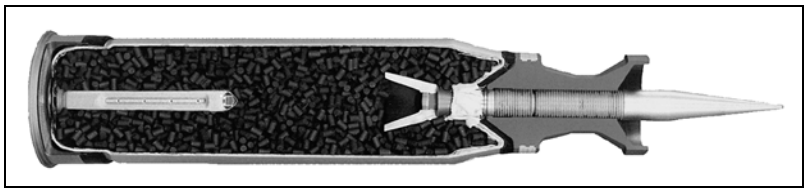

Figure 1. A cut away of large-caliber ammunition showing piccolo tube.

flow rate as a function of time and, in some cases, axial distance. This table can have both radial and axial dimensions and is usually obtained from a set of careful experiments (such as Chang and Rocchio [*12*]). This type of primer model includes solely the gas phase and ignores any ignition enhancement that may exist when hot burning particles are ejected from the igniter tube. Nevertheless, this type of primer model has been used successfully to predict the performance of a number of large-caliber U.S. Army guns (*6*, *13*, *14*).

Small-caliber ammunition (figure 2) is traditionally encased with a brass shell or casing; it has a metal jacketed lead projectile or bullet and has a ball powder propellant charge in the main chamber to discharge the projectile upon initiation from the pulling of the trigger.

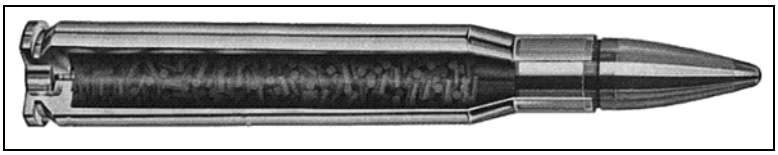

Figure 2. Cut away of a 5.56-mm small-caliber round.

The conventional ignition system for a small-caliber (for example, 5.56 ammunition; see figures 3 and 4) weapon consists of a metal cup primer (approximately 4.5 mm in diameter) with an interior anvil which when hit by a firing pin allows the ignited primer material to exit through the tubular primer flow channel (hereafter referred to as the flow channel) into the main chamber of the round and ignite the propellant charge (*15*). Conventional modeling of this primer charge system generally consists of a tabular input of igniter-gas mass flow rate as a function of time specified along a small radial region along the breechface. This table has solely a radial dimension. This type of primer model includes only the gas phase and ignores any charge ignition enhancement from ejected hot burning particles. It is widely recognized that this limited treatment of the small-caliber primer is not appropriate for IB modeling and has not been successfully used by anyone, to the authors' knowledge. Hot particles play an important role in the propellant ignition in small-caliber ammunition (*10*, *16*, *17* [page 66]). However, the present authors are unaware of hot particle enhancement of ignition being successfully implemented anywhere in the IB modeling literature.

Presented in this report is the development of a one-dimensional model of the small-caliber primer with the hope that the model can be later extended to the large-caliber configuration. The non-linear terms in the Navier-Stokes equations and the pressure term make turbulent fluid flows

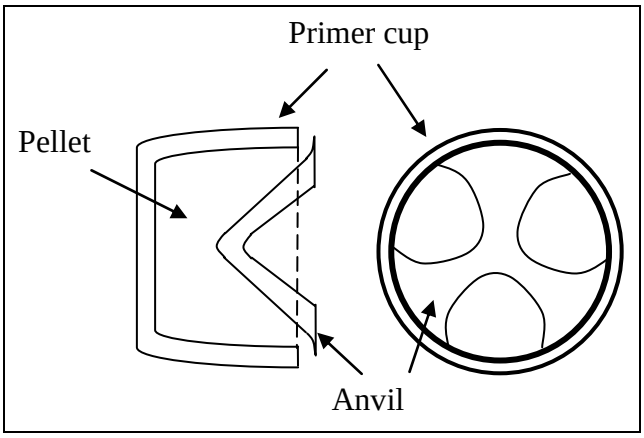

Figure 3. Small-caliber ammunition igniter; primer cup with anvil.

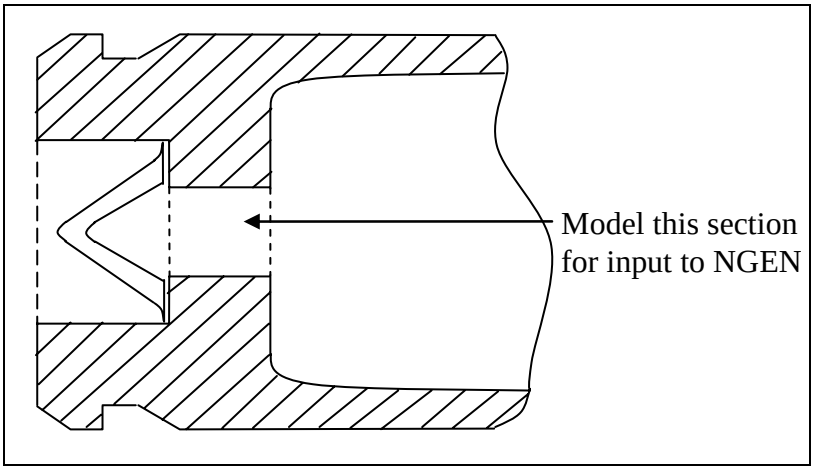

Figure 4. Axial cross-section schematic of primer for a 5.56 ammunition.

difficult to solve even on the fastest computers. With this in mind, people have made a varying number of simplifications commensurate with what their needs and available tools (such as computer speed) were. The model utilized in this report is based on a method of integrating the two-phase flow equations into the vector formulation of a One-Dimensional Turbulence (ODT) (*18*) model to simulate the flow channel which bridges the percussion primer and the propellant chamber in the 5.56 round (figure 4) as a steady-state particle-laden turbulent channel flow.

The novel ODT model is an unsteady turbulent flow simulation model implemented on a one-dimensional domain while preserving three velocity components, representing flow evolution as observed along a line of sight through a 3-D turbulent flow. Overturning motions representing individual eddies are implemented as instantaneous rearrangement events. They obey applicable conservation laws and emulate the multiplicative increase of strain and decrease of length scales associated with the turbulent cascade. Eddy occurrences are random, with likelihoods

proportional to a local measure of shear kinetic energy. These events punctuate conventional time advancement of viscous transport. The ODT model has been used successfully to simulate two-phase flow, one-way coupling, in a fully developed turbulent channel. Verification was achieved by comparison with direct numerical simulation (DNS), measurements, and large eddy simulation (LES) over a wide range of friction Reynolds ($180 \leq Re_\tau \leq 1200$) and a wide range of Stokes numbers, based on wall units, ($0.3 \leq St \leq 55{,}000$) (*19*).

Other methods such as LES, DNS, and Reynolds-Averaged Navier-Stokes (RANS) could be (and in many cases have been) applied successfully to solve similar two-phase flow problems.

Unlike LES, ODT would resolve the scales necessary to capture the smallest eddies in the one dimension (transverse to the flow) which ODT keeps track of. In addition, LES needs a subgrid model to account for energy losses due to such things as viscosity. Since ODT keeps track of the smallest eddy scales, the standard viscous dissipation equation takes care of this. An additional consideration is that the LES method would need a subgrid model to account properly for the two-phase flow portion of the model. Because ODT captures the smallest scales, no additional assumptions are needed for implementation into ODT. As Pope (*20*) points out, when defining LES as resolving 80% of the energy in the grid, the high turbulent Reynolds numbers are still beyond the reach of the largest main frames. (This Reynolds number boundary is continuously being moved higher.) To add to this restriction, the fact that particle-laden LES requires a significant increase in computer resources (over fluid only LES) indicates that ODT is an acceptable alternative to LES.

The state-of-the-art DNS modeling of turbulent flows is restricted by the maximum Re allowable due to the memory and speed of the fastest computers available. The memory requirement for DNS goes as the number of grid points needed to resolve fully the turbulent (Kolmogorov) scale raised to the third power. Since ODT keeps track of only one dimension, the required memory scales directly with the number of grid points needed to resolve the turbulent scale. Though progress to bring DNS to the high Re regime continues on all fronts, there is still much work to be done in order to use DNS for practical industrial or military applications. Since the ODT model capitalizes on the symmetry of the flow and utilizes innovative methods to model three-dimensional turbulent behavior on a one-dimensional domain, it is the model of choice for this highly turbulent flow configuration.

RANS based models have also been used to predict two-phase-flow problems (*21*). Call and Kennedy (*22*, *23*) have shown that stochastic separated RANS models do a poor job in capturing the behavior of evaporating droplets in turbulent flow. They suggest that the treatment of droplet vaporization may be problematic. The multi-physics involved (the coupling between the droplet evaporation, the drag, and the turbulent eddies on the droplet trajectory) indicates that the instantaneous gas temperature profile is also of primary importance when droplets are undergoing vaporization since the variations in the gas phase temperature directly correspond to variations in the droplet temperature profile. Since ODT keeps track of the instantaneous

velocity and temperature profiles, it has a distinct advantage in the long run over RANS, which does not automatically correlate the velocity and temperature fluctuations. There are authors who have attempted to add models which will do such correlations, but they do so by adding more models to the RANS structure. The present authors believe that working with ODT rather than RANS will make the results less model dependent.

In the present report, initial results are shown for the primer model run as a stand-alone code and are compared to the on-going experiments with small-caliber primers being conducted by Williams et al. (*24*). Some aspects of our work are compared to Kuo et al. (*25*). Plans for coupling the present primer model to the ARL-NGEN3 code and extensions of the model to large-caliber primers are discussed.

2. The ARL-NGEN3 IB Code

Since one of the primary motivations for the present work is to develop a primer model that is compatible with the ARL-NGEN3 IB code, a brief description of this code is included for completeness. For further details the reader is referred to papers by Gough (*4, 5*) and Nusca (*5, 6*).

The Army's NGEN3 code is a multi-dimensional, multi-phase CFD code that incorporates three-dimensional continuum equations along with auxiliary relations into a modular code structure. On a sufficiently small scale of resolution in both space and time, the components of the interior ballistic flow are represented by the balance equations for a multi-component reacting mixture describing the conservation of mass, momentum, and energy. A macroscopic representation of the flow is adopted using these equations derived by a formal averaging technique applied to the microscopic flow. These equations require a number of constitutive laws for closure including state equations, intergranular stresses, and interphase transfer. The numerical representation of these equations as well as the numerical solution thereof is based on a finite-volume discretization and high-order accurate, conservative numerical solution schemes. The spatial values of the dependent variables at each time step are determined by a numerical integration method denoted the continuum flow solver (CFS), which treats the continuous phase and certain of the discrete phases in an Eulerian fashion. The Flux-Corrected Transport scheme is a suitable basis for the CFS since the method is explicit and has been shown to adapt easily to massively parallel computer systems. The discrete phases are treated by a Lagrangian formulation, denoted the large particle integrator (LPI), which tracks the particles explicitly and smoothes discontinuities associated with boundaries between propellants yielding a continuous distribution of porosity over the entire domain. The manner of coupling between the CFS and the LPI is through the attribution of properties (e.g., porosity and mass generation). The size of the grid as well as the number of Lagrangian particles is user prescribed. The solid propellant is modeled using Lagrange particles that regress, produce combustion product gases, and respond to gasdynamic and physical forces. Individual grains, sticks, slab, and wrap layers are not resolved;

rather, each propellant medium is distributed within a specified region in the gun chamber. The constitutive laws that describe interphase drag, form-function, etc., assigned to these various media determine preferred gas flow paths through the media (e.g., radial for disks and axial for wraps) and responses of the media to gasdynamic forces. Media regions that are encased in impermeable boundaries which only yield to gasdynamic flow after a prescribed pressure load is reached act as rigid bodies within the chamber. The use of computational particles to represent the propellant charge permits a host of other modeling features that enhanced the representation of charge details.

3. Description of the Primer

3.1 Chemistry

The composition of Army small-caliber primers is well known (*15*) and unchanged for many years (table 1). This primer composition is used in all of the Army's small- and medium-caliber ammunition.

Table 1. Chemical composition of the number 41 primer mixture.

Name	Formula	Weight-Percent	± Weight-Percent Deviation	Primary Purpose
Lead styphnate	$H_3 C_6 N_3 O_9 Pb$	37	5	Primary explosive
Barium nitrate	$Ba (N O_3)_2$	32	5	Oxidizer
Antimony sulfide	$Sb_2 S_3$	15	2	Fuel, slow
Aluminum powder	Al	07	1	Fuel, fast
Tetracene	$H_8 C_2 N_{10} O$	04	1	Primary explosive
PETN	$C_5 H_8 N_4 O_{12}$	05	1	High explosive

Lawrence Livermore National Labs developed a thermodynamics code for explosives called Cheetah (*26*) which includes the option for a gun calculation. The gun calculation is done under conditions of constant specific volume and enthalpy, which are meant to simulate a gun firing. Of special interest to the IB community is the ratio of specific heats (frozen) called γ, along with the thermodynamically predicted temperature and pressure.

Primary explosives detonate or explode upon shock or added heat. High explosives detonate under the influence of the shock of the explosion of a suitable primary explosive. Explosives do not necessarily combust; in some cases, explosives do not have the necessary ingredients to combust. Propellants are materials which contain sufficient amount of oxygen to burn without exploding, but provide gas which thereafter may produce an explosion. Fuels are similar to propellants, but they need oxygen from another source to burn. Oxidizers are materials with excess oxygen which when liberated can be used by a fuel.

The lead styphnate and tetracene are primary explosives meant to convert the shock induced by the firing pin into the initiation of the primer material. Tetracene is the more impact sensitive of the two (*10, 27*) and is important in order to keep stability in the sensitivity of the small-caliber primer (*28*). Davis (*10*) points out that as little as 2 weight-percent is enough to improve the sensitivity of primers. The impact sensitivity of tetracene is given as 1 N-m, and lead styphnate as 2.5–5 N-m (27).

The PETN (pentaerythritoltetranitrate) is a high explosive added to the primer mix to increase brisance (the shock produced) and heat produced. The impact sensitivity is given as 3 N-m (*27*).

The aluminum powder increases the heat produced upon ignition, i.e., the enthalpy of combustion of aluminum raises the peak temperature of the explosive event. (The added effect is dependent on the Al particle size.) The aluminum powder is assumed to sequentially oxidize, but first the encapsulating Al_2O_3 coating must be disturbed to allow oxygen to the elemental Al in the core of the powder. This can be done by melting the oxide (2045 °C, melting point), melting the interior elemental Al (660 °C, melting point), or vaporizing the interior Al (2057 °C, boiling point). It is interesting to note that an explosive mixture consisting of only liquid oxygen and porous aluminum was invented in 1895 (*10*, page 355), the products of which are only solid aluminum oxide, the excess oxygen gas, and much heat. The aluminum powder is a fuel which burns quickly once ignited due to a cascading effect of the large amount of heat released.

The barium nitrate is an oxidizer which undergoes a chain of decomposition reactions which first produce NO_x and barium peroxide. The NO_x goes into the gas phase where it can supply oxygen to the fuels. The barium peroxide decomposes to barium oxide with further heating during the primer initiation. Barium nitrate produces a green flame when burned in air.

$$Ba(NO_3)_{2(S)} \xrightarrow{heat} BaO_{2(S)} + 2NO_{X(G)}. \quad (1)$$

$$BaO_{2(S)} \xrightarrow{heat} BaO_{(S)} + \frac{1}{2}O_{2(G)}. \quad (2)$$

The antimony sulfide, also known as stibnite, is a slow fuel. Davis (*10*, page 454) describes, as an constituent of percussion primers, "antimony sulfide (a combustible material which maintains the flame for a longer time) …" Antimony sulfide produces a blue flame when burned in air.

3.2 Description of the Primer Firing Event

The action of the firing pin hitting the primer cup causes the detonation of the primary explosives (tetracene and lead styphnate) and the high explosive (PETN). The aluminum is a fuel which burns very quickly. The outer surface of the Al powder is actually Al_2O_3, up to 30 % by weight. Burning occurs when the inner Al (that is not oxidized) is exposed to oxygen. This can be done by either melting the solid particles or vaporizing it (sublimation). Oxide cracking would also provide an avenue for oxygen to reach the aluminum. The convection currents in the melted Al particles would assure fresh un-oxidized aluminum would be supplied to the surface. Once at the

surface it would react with available oxygen and release a generous amount of heat. This heat would increase the convection currents supplying more un-oxidized aluminum at the surface, and a cascading effect takes place. After a suitable amount of energy is produced by this process the particles could then vaporize, which would burn (oxidize) in the vapor phase. The first reaction of aluminum with oxygen produces AlO. The largest spectral signature from burning aluminum powder is Al O (*29*).

$$Al + \frac{1}{2} O_2 \rightarrow Al\,O\,. \tag{3}$$

From the open-air experiments and analysis of Williams et al. (*24*), the aluminum containing particles are mostly in the submicron size range. This indicates that the aluminum containing particles nucleated from the vapor phase into the solid phase upon cooling. This supports the supposition that the aluminum powder is a fast burning fuel.

The barium nitrate is an oxidizer with the primary purpose of ensuring that the fuels have enough oxygen containing compounds in the vapor phase to react to completion. The decomposition of barium nitrate is highly endothermic (*17*, page 263) and burns with a green flame (*30*, page 29). The decomposition process is described in detail by Bordon and Campbell (*31*). As previously stated, the barium nitrate decomposes with heat to oxygen containing nitrogen compounds which can then give up their oxygen in the gas phase. The barium peroxide will (with additional heating) decompose to barium oxide and oxygen. The oxygen is then available for the fuels in the gas phase. The analysis (*24*) indicates that there may be some BaO present after the open air firings, but that was inconclusive. Kaste's analysis of the products of the closed chamber packed with inert propellant grains, primer firing showed a marked decrease in the nitrates. This is consistent with the higher pressure, temperature, and time of exposure to which the primer products (including barium nitrate) would be exposed in a closed chamber with an inert propellant bed.

The antimony sulfide is also a fuel similar to the aluminum powder, but the reaction takes a longer time. The solid antimony sulfide melts with added heat; the liquid drops must absorb more heat to vaporize, only once it reaches the vapor phase can the antimony sulfide produce appreciable amounts of antimony oxide. The analysis of both the open air and inert propellant experiments of Williams et al. (*24*) indicates that this reaction is slow, as no antimony oxide peaks were detected by Fourier Transform InfraRed (FTIR), which would have been readily apparent if there were any substantial amounts. It is possible that the antimony sulfide also serves a secondary purpose during the initiation phase of the primer. That is while the firing pin is impinging on the primer cup, the secondary purpose is to make the mixture more sensitive to percussion. A similar function is provided by ground glass in some percussion primers (*10*, page 455). Of note is that high-speed films of the no. 41 primer open air firings (*24*) were compared to the open air firings of a primer without antimony sulfide as an ingredient. The primer no. 41 firing showed a definite blue hue near the end of the firing event, where the primer without stibnite failed to show a blue hue. This indicates that there was some burning of the antimony sulfide.

For the present work, the proposed model is that the primary and high explosives detonate first, with the aluminum powder burning quickly after. The barium nitrate decomposes after some heating, which takes longer than the aluminum. The antimony sulfide first melts and vaporizes before it can react, which takes the longest time due to heat transfer and kinetic constraints.

In order to properly supply the NGEN code with information on the efflux from the primer spit hole (see figure 4), we propose that particles of barium nitrate and antimony sulfide are heated in the flow channel. The flow channel is represented by a particle-laden fully turbulent channel flow. Some of these particles melt due to heat conduction from the hot turbulent gas flow through the primer flow channel produced in the detonation event.

Gun thermodynamic calculations were performed using the Cheetah code (*26*) with the components tetracene, lead styphnate, PETN, and aluminum powder to simulate the gas phase equilibrium conditions. The aluminum powder was assumed to be 30% by weight Al_2O_3 and the balance elemental Al. The results can be found in table 2. In this model, the stibnite and barium nitrate are only heat sinks (absorbing energy from the flow) while in the primer tube. To account for the heat loss, an estimate of energy needed to bring these solid particles from room temperature to the thermodynamically determined final temperature (as predicted by a Cheetah gun calculation) was subtracted from the heat of formation of one of the components (lead styphnate). Only some of the heat capacities and heats of fusion for barium nitrate and antimony sulfide were available in the literature. Utilizing the heat capacity of solid stibnite, the amount of energy needed to take the compound from room temperature to its melting temperature of 819 K was calculated. The heat of fusion (33 cal/g) was then used to compute the heat necessary to melt the stibnite. The heat capacity of liquid antimony sulfide could not be found. As an approximation, the heat capacity of liquid antimony was used in its stead. Therefore, an estimate of the energy necessary to bring antimony sulfide from room temperature to 2312 K was computed. The energy needed to heat the barium nitrate was assumed to be identical. The experimental observations (*24*) and the Cheetah calculations both indicate that the flow inside the primer tube is highly turbulent. The gun calculation was done with a loading density of 0.0139 g/cm^3. This was computed from the mean pellet weight (0.025 g) as specified in the military drawing M855TDP for the 5.56 primer pellet and the empty chamber volume of 1.8 cm^3. The input and output files for Cheetah can be found in the appendix. Based on the assumption that the stibnite and barium nitrate remain in the solid phase and the condensed phase from the Cheetah calculation, this model estimates a condensed phase of greater than 60%. Note that this is inconsistent with the Kuo et al. (*25*) computed estimate of 40% condensed phase.

Table 2. Cheetah code gun calculation results.

Temperature	Pressure	Impetus	Molecular Weight	Covolume	Gamma, Frozen
2797 K	7.4 MPa	530 J/g	44 g/g-mol	0.635 cm^3/g	1.176

4. Formulation of the Primer Model

The pertinent work of Williams et al. (*24*) as related to this primer model consisted of a set of open-air primer experiments recorded with time-lapse photography and analysis of the blast via a witness plate and subsequent SEM/EDAX/FTIR analysis. Additional experiments were performed in a closed chamber with inert balls meant to simulate the primer action as realistically as possible without the ignition of a propellant bed.

A fundamental motivation behind the production of this model is the conjecture that the hot particles ejected into the propellant bed are essential to capturing the initiation and flame spreading phenomena.

The pictures indicate that the explosion event consists of hot gases and particles being ejected from the flow channel at high velocities. This motivated the development of a primer model concentrating on the flow channel. With proper attention to detail, the output of this primer tube can be feed into the NGEN code. NGEN calculations can then be made to carry these gases and particles to the proper ignition of the propellant bed with minimal changes to NGEN.

The primer tube is modeled as a fully turbulent steady-state particle-laden fluid channel flow. The particles are chosen to be $Ba(NO_3)_2$ and Sb_2S_3 based on the thermochemical calculations and the results from Williams et al. (*24*). Particles are released into the simulation of the flow channel at room temperature and allowed to absorb heat from the turbulent channel. Upon heating the particles melt. The hot particles which leave the spit hole are carried by the NGEN simulation into the propellant bed (see figure 4). There they release heat conductively to the propellant and can aid or even cause ignition of the propellant.

4.1 The Navier-Stokes Equation

$$\rho \frac{D\tilde{u}}{Dt} = -\nabla P + \mu \nabla^2 \tilde{u} + \rho \tilde{g} \, . \tag{4}$$

The Navier-Stokes equation simply says that the mass per unit volume times the acceleration (which is the Left Hand Side [LHS]) is equal to the pressure force on said element per unit volume (first term on the Right Hand Side [RHS]) along with the viscous force on the element per unit volume plus the body forces per unit volume (the last term on the RHS). Note that even though g is used, equation 4 is not restricted to only gravitational forces. Vectors are denoted by a tilde "~" above, ρ is the density of the fluid, μ is the viscosity, P is the pressure, t is time, and u is the fluid velocity vector.

4.2 Overview of the One-Dimensional Turbulence Model

Kerstein developed a one-dimensional Monte Carlo modeling technique for turbulent mixing of velocity and scalar fields. A subsequent extension (*18*) keeps three velocity components on the ODT domain. This allows for the introduction of an ODT analogy of pressure scrambling. The fields defined on the one-dimensional domain evolve by two mechanisms: molecular diffusion and a stochastic process representing advection. The ODT approach represents turbulent advection by a random sequence of "eddy" maps applied to a one-dimensional computational domain. Profiles of the velocity components (u_i) and the advected scalars evolve on this domain. Equations for the turbulent flow field are not solved explicitly; rather, the viscous and diffusive equations are solved:

$$\frac{\partial u_i(y,t)}{\partial t} = \nu \frac{\partial^2 u_i(y,t)}{\partial y^2} - \frac{1}{\rho}\frac{dp}{dx} \quad , \quad \frac{\partial \theta(y,t)}{\partial t} = \kappa \frac{\partial^2 \theta(y,t)}{\partial y^2}, \tag{5}$$

where t is time, ν is the kinematic viscosity, ρ is the density, θ can be any advected scalar (e.g., temperature, species concentration, etc.), and κ is the corresponding diffusion coefficient. Note that the dp/dx term in equation 5 is an imposed mean pressure gradient in the streamwise direction.

In order for ODT to be used there must be a minimum of one homogeneous direction. There should be a predominantly streamwise direction. The one dimension in the ODT model is transverse to the mean flow. The ODT model implements triplet maps or eddies as instantaneous rearrangements of the velocity $u_i(y, t)$ field.

The events representing advection may be interpreted as the model analogue of individual turbulent eddies. However, this interpretation is not essential to the analysis; it merely provides an intuitive basis for presenting the model. Essentially, each 'eddy event' has three properties: a length scale l, a time scale τ, and a measure of kinetic energy.

The vector (three-component) form of ODT has eddy events consisting of two mathematical operations. The first is a measure-preserving map representing the fluid motions of a turbulent eddy. The other is a modification of the velocity profiles in order to account for energy transfers between velocity components.

$$u_i(y) \to u_i(f(y)) + c_i K(y), \quad \theta(y) \to \theta(f(y)). \tag{6}$$

The fluid at location $f(y)$ is moved to location y by the mapping operation. This mapping is the vector ODT analog of the advection operator $v \cdot \nabla$ of the Navier-Stokes equations. This mapping is applied to all fluid properties. The additional term $c_i K(y)$, which is only applied to the velocity components, is the ODT analogue of pressure-induced energy redistribution among the velocity components. This also takes care of velocity changes due to pressure gradients or body forces.

The triplet map has a starting point y_o and a length l which are sampled randomly from an eddy distribution rate. The mapping rule $y \rightarrow \bar{y}$ for a triplet map is given by

$$\bar{y} = \begin{cases} y_o + \frac{1}{3}(y - y_o) & y_o < \bar{y} < y_o + \frac{1}{3}l \\ y_o + \frac{2}{3}l - \frac{1}{3}(y - y_o) & y_o + \frac{1}{3}l < \bar{y} < y_o + \frac{2}{3}l \\ y_o + \frac{2}{3}l + \frac{1}{3}(y - y_o) & y_o + \frac{2}{3}l < \bar{y} < y_o + l \\ y & otherwise \end{cases}, \quad (7)$$

where $\bar{y}$ is the y profile after the instantaneous rearrangement.

The desired attribute of the triplet map is to provide a means of mimicking the increase in strain intensity, the decrease in strain length scale, and the increase in mixing due to eddies in physical turbulent flow. This mapping rule assures that closest neighbors after the spatially discretized mapping event were no more then three cells (or fluid elements) apart before the mapping event. Hence, the increased strain rate and shortening length scale is attained without undue introduction of discontinuities. Using the continuous analog to describe the triplet map, the original scalar profile is reduced by a factor of three, and a copy is placed in both the first third and the last third of the eddy domain. For the middle third, the reduced image is inverted.

Though there are other mappings which could be used, this implementation of the triplet map is the simplest which obeys three key physical conditions: (1) measure preservation (the non-local analog of vanishing velocity divergence, this property is manifestly satisfied in the discrete numerical implementation, in which the map is a permutation of equal-volume fluid cells on the 1D domain), (2) continuity (no introduction of discontinuities by the mapping operation), and (3) scale locality (at most order-unity changes in property gradients). The first two conditions are fundamental properties of incompressible fluid motion. The third is based on the principle that length-scale reduction in a turbulent cascade occurs by a sequence of small steps (corresponding to turbulent eddies), causing down-scale energy transfer to be effectively local in wavenumber.

Fluid parcels or elements are moved instantaneously during the triplet map from one y location to another. The momentum and passive scalar properties of each fluid particle or cell are preserved and remain unaffected (at first) by the instantaneous rearrangement. Subsequently energy redistribution among the three velocity components is implemented. This is represented by the c_i term in equation 6. In equation 6, the K term is a kernel function that is defined as $K(y) = y - f(y)$. Hence, its value is equal to the distance the local fluid element is displaced. Therefore, it is by definition non-zero only within the eddy interval l. The kernel integrates to zero so that the 'eddy event' does not change the total (y-integrated) momentum of individual velocity components.

As mentioned, each eddy event has a time, a length scale, and a measure of kinetic energy associated with it. The kinetic energy of an individual velocity component *i* is

$$E_i \equiv \tfrac{1}{2}\rho\int u_i^2(y)dy\,. \tag{8}$$

(The density ρ, assumed constant, is defined here as mass per unit length.) The amplitudes c_i in equation 6 are determined for each individual eddy subject to two constraints: (1) the total kinetic energy remains constant and (2) the energy removed from any individual velocity component by the kernel mechanism cannot exceed the energy available for extraction (*18*).

In ODT, eddy events are instantaneous in time and occur with frequencies comparable to the turnover frequencies of corresponding turbulent eddies. Events are therefore determined by sampling from an event-rate distribution that reflects the physics governing eddy turnovers.

Flow properties (e.g., velocity variations) affect the eddy rate distribution and the successful eddy events (based on sampling using a rejection method) affect the velocity distribution (and passive scalars). This creates a feedback by increasing the strain rate which allows more triplet maps to occur. The event rate, λ, is shown (*18*) to be

$$\lambda(y_o,l;t) \equiv \frac{C}{l^2\tau(y_o,l;t)} = \frac{C\nu}{l^4}\sqrt{\left(\frac{u_{2,K}l}{\nu}\right)^2 + \alpha\sum_j T_{2,j}\left(\frac{u_{j,K}l}{\nu}\right)^2 - Z}\,, \tag{9}$$

where the matrix *T* assures invariance under axis rotation; all other new variables are defined shortly. If the quantity in the radical of equation 9 is negative, the eddy is deemed to be suppressed by viscous damping and λ is taken to be zero for that eddy. In the square root term, the quantities preceding *Z* involve groups that have the form of a Reynolds number. As such, *Z* can be viewed as a parameter controlling the critical Reynolds number for eddy turnover.

There are three free parameters in the ODT model proper: *C*, α, and *Z*. The free parameter *C* determines the strength of the turbulence; hence, *C* allows fine adjustments to the eddy rate distribution. The transfer coefficient α determines the degree of kinetic energy exchange among components. (The matrix *T* in equation 9 depends on α.) The viscous cutoff parameter *Z* determines the smallest eddy size for given local strain conditions.

These three parameters, along with the initial and boundary conditions of the flow and the physical conditions of the fluid (density, viscosity, etc.), constitute the complete inputs for the vector ODT model proper. One additional free parameter is needed for the two-phase flow application.

4.3 Particle Dynamics for a Perfect Sphere

The full equation of motion for a particle suspended in a fluid (*32*):

$$\frac{\rho_p \pi}{6} D_p^3 \frac{d\tilde{V}}{dt} = 3\pi\mu D_p \left(\tilde{u} - \tilde{V}\right) + \frac{\pi}{6} D_p^3 \rho_f \frac{d\tilde{u}}{dt} + \frac{\pi D_p^3 \rho_f}{12}\left(\frac{d\tilde{u}}{dt} - \frac{d\tilde{V}}{dt}\right) + \frac{3D_p^2}{2}\sqrt{\pi\rho_f \mu}\int_0^t \frac{\left(d\tilde{u}/dt'\right) - \left(d\tilde{V}/dt'\right)}{\sqrt{t-t'}} dt' + \sum_i F_{ei}, \tag{10}$$

where the LHS is the mass times the acceleration term, or the change in particle inertia. The first term on the RHS is Stokes force due to viscous drag. The second term on the RHS is due to pressure gradient in the fluid surrounding the particle, caused by acceleration of the gas by the particle. The third term on the RHS is the force required to accelerate the apparent mass of the particle relative to the fluid (that is the "added mass" term, the force needed to accelerate the fluid displaced by the sphere). The fourth term on the RHS is called the Basset history integral; this accounts for the force arising due to the deviation of the fluid velocity from steady state (or one can view this as accounting for the increase in viscous drag due to flow unsteadiness). The fifth and last term on the RHS is simply the summation of the body forces, or the buoyancy forces. Note that the particle velocity vector is *V*, the subscript *p* is a for particle property, the subscript *f* is for a fluid property, and D_p is the diameter of the particle.

This equation has a long history (see Stock [*33*]) and is known as the BBO equation, for Bassett-Boussinesq-Oseen equation (see Maxey and Riley [*34*]). It is the general Lagrangian equation of motion for particles in an unsteady flow.

Luckily, many of the terms drop out if the density of the particle is much greater than the density of the air, as long as the diameter of the particle stays below the smallest turbulent eddy scale. This equation can be simplified to equation 11 (*35*). Note that equation 11 can also be derived by a simple force balance around a particle. The drag law, equation 11, may seem too simple when compared to equation 10, but Sirignano (*36*) states that good engineering analysis can be performed using only modified Stokes drag and the gravitational force. A majority of the state-of-the-art publications in the area of two-phase flow use the simplified drag force to compute the motion of particles.

$$\frac{d\tilde{V}}{dt} = \frac{\tilde{F}_G}{m_p} + \left(\tilde{u} - \tilde{V}\right)\frac{f}{\tau_p}, \qquad \frac{d\tilde{X}}{dt} = \tilde{V}, \tag{11}$$

$$\tau_p = \frac{\rho_p D_p^2}{18\mu}, \quad f = \begin{cases} 1 & Stokes\ law \\ 1 + 0.15\,\mathrm{Re}^{0.687} & non-linear \end{cases}, \quad \mathrm{Re} = \frac{\rho_g r_p \left|\tilde{V}_p - \tilde{u}_g\right|}{\mu_g}. \tag{12}$$

4.4 Particle – Fluid Interactions

The development of two-phase flow models with a turbulent gas phase is traditionally broken into three categories: one-way coupling, two-way coupling, and four-way coupling. The simplest is one-way coupling, or passive particle transport. In one-way coupling the turbulent contribution of the dispersed phase is negligible. The turbulent field is much more likely to gain kinetic energy from the gas flow rather than from the flow of the dispersed phase. Here, the fluid affects the particle, but the particle does not affect the fluid. This is often symbolized as follows: fluid → particle (one arrow).

The two-way coupling flows are the next complicated. In this case the volume fraction of the dispersed phase is high enough that the mean flow of the particles can induce turbulent motion in the fluid. (Also, as in the one-way coupling, the turbulent fluid motion induces motion in the particles. Hence the title, two-way coupling.) This is symbolized as follows: fluid ← → particle (two arrows).

The most complicated of the flows is referred to as four-way coupling. In this case, the volume fraction of the dispersed phase is so large that the dispersed phase particles not only affect the fluid flow, but also affect each other by way of collisions or near collisions (wake or boundary layer interactions). This is symbolized as follows: fluid ← → particle ← → particle (four arrows). Elghobashi (*37*, *38*) shows the range in which the three types of coupling are of importance.

The present model utilizes the one-way coupling, or passive transport assumption. A Lagrangian framework for the particle is used with the key forces on the particle considered to be a modified Stokes drag and gravity. A majority of the state-of-the-art publications in the area of two-phase flow use the one-way coupling assumption along with a drag force to compute the equation of motion of particles.

4.5 Particle – Wall Interactions

In real world experiments (such as the flow in the primer firing), there are many contributing factors which make the two-phase flow modeling a difficult task. A short discussion on some of the main points of consideration when modeling particle-wall interactions is here presented.

The main considerations for collisions are elastic vs. inelastic and all particles bouncing off vs. all particles sticking to the wall vs. some combination of any of these. There are other important considerations, such as (1) what happens if the particles are nonspherical (*39*) (will wall collisions cause the particles to spin and hence create Magnus forces), (2) the difference between free slip and no slip surfaces (*40*), and (3) re-entrainment mechanisms in turbulent flow as a function of particle size (*41*), to name but a few, but these are left for future work.

A particle which hits a surface in the real world would either bounce off or stick to the surface. It must do one or the other, unless the particle somehow breaks apart and one part sticks to the

wall while the other is re-entrained into the fluid flow. For obvious reasons, particle break up is too complicated for the scope of the present project.

Particles which hit the wall and bounce off are most likely affected by the wall roughness. Many experimenters go to great pains to make the surfaces smooth relative to the particle size they are interested in or to characterize the surface roughness.

Particles which bounce off a surface are not only affected by the roughness of the wall, but they also bounce off in an inelastic manner. Many surfaces, however, can closely match the behavior of flat walls with totally elastic collisions for all practical purposes.

For the present work all collisions with a wall stick to the wall. For future work, the determination is based on the physical state of the particles: if a particle is in the solid phase, it bounces off the wall; if a particle is in a liquid phase, it sticks to the wall. This, of course, cannot hope to totally capture real experiments, since real experiments have much more physics than either of these two cases. Note however that many researchers use spectral reflection (*42–44*) for studying particle behavior in turbulent channel flow. Many other researchers investigate turbulent particle deposition by particles sticking to the wall as soon they get within one particle radius of the wall (*45–49*).

4.6 Model Implementation

To implement particle-laden flow into ODT is not straightforward because fluid motion (displacement by eddy events) and fluid velocity are distinct in ODT. This problem was first overcome by Schmidt (*50*), where a particle-eddy interaction mechanism was introduced. The net outcome is a particle-eddy interaction that obeys correct limiting behaviors (infinite inertia and vanishing inertia) and transitions smoothly between these limits. A second difficulty arises because the fluid velocities are being tracked in a Eularian reference frame but the particles are tracked in a Lagrangian reference frame. If the velocity of the particle is much greater than the bulk velocity of the fluid, the particle would move a distance X downstream in a much shorter time than the flow would move that same distance. This is compensated for by setting the particle time line to account for the velocity difference between the particle and the fluid.

The particle-fluid interaction during continuous evolution follows conventional approaches to drag law implementation, except that (1) to preserve the tracer limit only the x and y components of the gas velocity are nonzero and (2) to preserve proper time development of the particle, particle time is set equal to continuous time, t, divided by one plus the slip velocity in the x direction divided by the bulk fluid velocity also called the plug flow velocity:

$$t_p = \frac{t}{1+\frac{|V_1 - u_1|}{U_{pf}}}. \tag{13}$$

Particle interaction with a triplet map requires a novel approach, albeit in the spirit of existing particle-eddy interaction models. This interaction occurs when the particle and triplet map occupy the same space-time. The particle drag law as written is not applicable to ODT particle-eddy interactions because triplet maps are instantaneous in time, yet the particle-drag law requires an interaction time to cause a change in the particle velocity or position.

The logical solution to this difficulty is to assign an interaction time to the particle-eddy interaction. The interaction time coordinate is called *T*. This coordinate is introduced so that the particle drag law can have an effect on the particle without time advancing the flow solution. Particle evolution during this interaction is governed by the *y*, *x*, and *z* components of the particle drag law recast as follows:

$$\frac{dV_2}{dT} = -\frac{\left(V_2 - v_E\right)}{\tau_p} f + A_{Gy}\,, \quad \frac{dV_1}{dT} = -\frac{\left(V_1 - u_1\right)}{\tau_p} f + A_{Gx}\,, \quad \frac{dV_3}{dT} = -\frac{\left(V_3 - u_3\right)}{\tau_p} f + A_{Gz}\,; \quad (14)$$

where T is the interaction time coordinate; v_E is the fluid y component velocity induced by the triplet map; u_1 and u_3 are the x and z velocity components of the fluid cell which contains the particle center at the onset of the particle-eddy interaction; A_{Gx} , A_{Gy}, and A_{Gz} are the accelerations due to all body forces in the x, y, and z directions; and all other terms are as previously defined. In this formulation, v_E is defined so that tracer particles behave correctly; that is, they mimic the motion of the fluid cell which surrounds them.

ODT proper has a time scale associated with every eddy $\tau(y_o, l; t)$. Accordingly, the eddy lifetime is taken to be a constant times that eddy timescale. The definition chosen for v_E is

$$v_E = \frac{h}{\beta\tau\left(y_o, l; t\right)}, \quad (15)$$

where h is the displacement of a fluid element and a free parameter β has been introduced. This definition is chosen because it yields the correct tracer-particle limit of equation 14.

As discussed in Kerstein et al. (*18*), in the analytical formulation of the triplet map, three images of the original fluid interval are formed, so there are three distinct fluid displacements h corresponding to the three images generated by the triplet map. For the fluid, the three displacements correspond to subdivision of a given fluid element into thirds, with application of a different displacement to each third. Unlike fluid elements, individual particles cannot be subdivided, so determination of v_E requires a determination of which one of the three h values associated with a fluid element applies to a given particle within the fluid element. The h for a particle is determined randomly from among the three choices.

An eddy exists in a defined space (three-dimensional) space for a defined lifetime. Particle-eddy interactions occur while the particle occupies the same space-time (x, y, z, t) as the eddy and ceases the first time the particle leaves the ODT space time (x, y, z, t), which the eddy is idealized to occupy. Additional details on this aspect can be found in Schmidt (*19*).

A problem arises when comparing the integration done in interaction time over a time period T and the conventional particle-time integration of the drag law subsequent to the particle-eddy interaction over a comparable time interval Δt. Comparison of equations 11 and 14 indicates that the equations contain similar terms and therefore the resultant actions of integrating them over the same time period are in fact double counting acceleration effects. To overcome this problem, the particle trajectories with and without the effect of the eddy are computed. This is achieved by integrating both during continuous evolution and interaction time concurrently over the period T and determining the difference in the ending y_p position and the ending V velocities.

$$\Delta y_p = y_p^i(T) - y_p^n(T), \quad \Delta V = V^i(T) - V^n(T). \tag{16}$$

These computations define the perturbations felt by the particle due to the eddy, where the superscript *i* (for interaction) denotes the results based on equation 14 and the superscript *n* (for no interaction) denotes using equation 11.

This procedure is pictorially represented in figure 5a. The perturbation distance, Δy_p, (demarcated with a "}") and the perturbation velocity, ΔV, are then added to the particle's original position and velocity (respectively) at the instant it first encounters the triplet map. On this basis, the particle location y_p' and y velocity V' resulting from the particle-eddy interaction are $y_p' = y_p + \Delta y_p$, $V' = V_2 + \Delta V$, where y_p and V_2 are the values at the instant the particle encounters the eddy (prior to the interaction). With double counting thus eliminated, continuous evolution resumes. Results of this procedure are shown in figure 5b. No adjustments in x_p, z_p, V_1, or V_3 are made for a particle-eddy interaction. Since interaction time exists only during particle-eddy interactions, the initial particle velocity, V_o, during interaction time is set equal to the final particle V_3 velocity from the last time that the particular particle was involved in a particle-eddy interaction. That way V_o matches the end V_3 velocity of that same particle the instant it ended the last particle-eddy interaction.

5. Computational Results for a Small-Caliber Simulator

Returning to the problem at hand, recall that figure 4 highlights the channel separating the primer from the main chamber of the ammunition.

The channel half height h was taken to be equal to the nominal radius of the primer flow channel tube as given in the military technical description package M855TDP as 0.1016 cm with a deviation of 0.00508 cm, which gives a cross-sectional area of 3.24×10^{-6} m^2.

The channel length is taken to be the equivalent length based on the volume if the primer chamber did not undergo a sudden contraction.

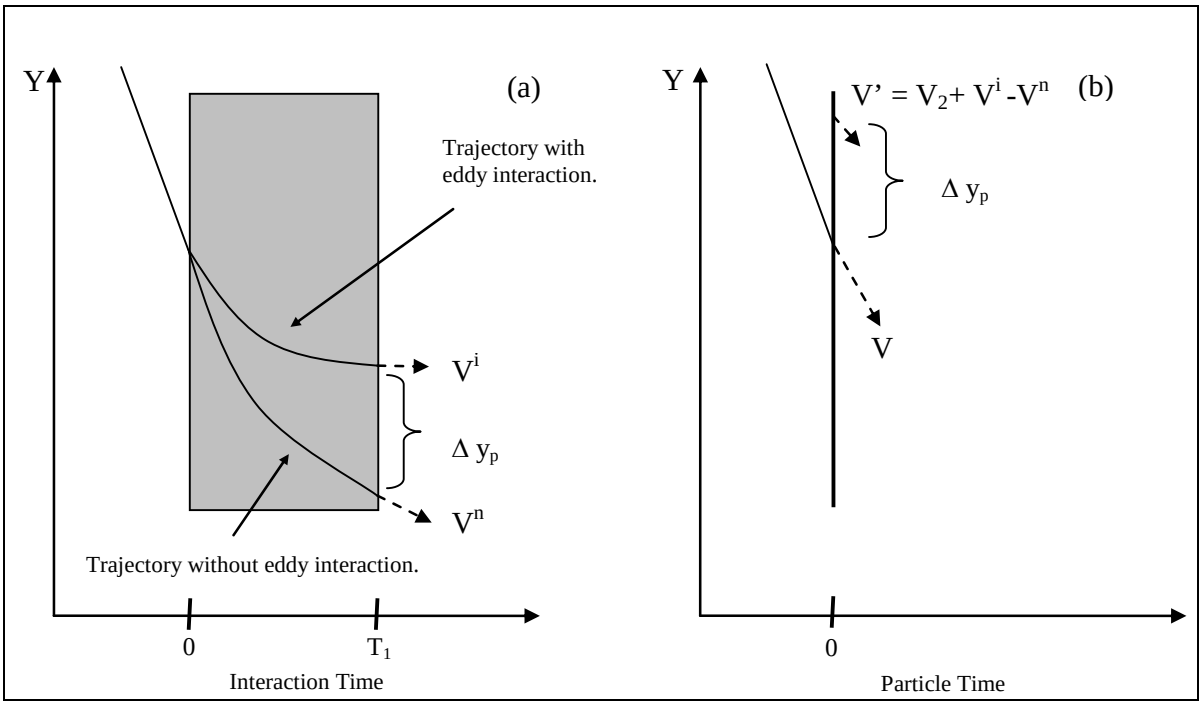

Figure 5. The procedure for implementing particle-eddy interactions which avoids double counting. Find Δy_p and ΔV, then add them to the original position and velocity. The resultant position and velocity are shown in (b).

Particle sizes are taken as a nominal size based on the military specification for the raw materials (stibnite and barium nitrate) used in preparation of the no. 41 primer. Particle distributions are possible, but left to future work.

Presently, all particles are released into the channel at the same instant in time. However, staggering the release time can be done easily, but is left to future work.

5.1 Parametric Scaling

In order to completely capture particle-laden channel flow in a computer simulation there needs to be dimensional similarity in the Reynolds number of the flow, the Stokes number of the particle, and the ratio of radius of the particles to the channel height *h*. In addition, the initial and boundary conditions of the fluid and the particles must be the same. Particle-laden ODT (PODT) is capable of meeting all of these conditions.

The bulk Reynolds number of the flow through the primer tube was computed by equation 17 with the (incompressible fluid) plug flow or bulk velocity U_{pf} defined in equation 18. The volume of the chamber V_c (1.5 cm^3) and the duration of the primer firing event *t* (9.55 ms) was taken from Williams (*51*) . This gave a plug flow velocity of ~ 48.4 m/s. The viscosity of the fluid is unknown; an estimate was taken by searching the thermophysical properties of compressed air in the region given by the Cheetah code (2800 K and 7.4 MPa) and looking for agreement with the density (0.12 kg/m^3). Reasonable agreement with the density was found in

the area between 6 and 8 MPa and 2500 K. A value of 8.17×10^{-5} kg/m/s was estimated for the primer products. This leads to a bulk Re ~ 12,000.

$$\mathrm{Re} = \frac{\rho_f \, U_{pf} \, D}{\mu_f}. \tag{17}$$

$$U_{pf} = \frac{V_c}{t * (cross - sectional\ area)}. \tag{18}$$

The properties of compressed air were used in a fully developed ODT channel flow simulation to obtain a mean flow velocity of 48 m/s. This was considered close enough to the 48.4 m/s previously calculated. Particles representative of stibnite particles were put into the simulation, utilizing a Stokes drag law (equations 11 and 12) with the gravitational force set to zero, and allowed to reach pseudo-steady-state. When particles travel to within one radius of the wall they were allowed to deposit on the wall. The average of all particle streamwise velocities were taken and found to be just over 47.5 m/s. Williams et al. (*24*) gives a measured value of 45 m/s. This was considered good agreement.

It is well known that near the wall the kinematic viscosity ν and the wall shear stress τ_w are important parameters of the flow. A time scale, called wall time t^+, can be defined from these and the fluid density (see equation 19). The Stokes number τ_p^+, as defined by equation 20, relates the relative importance of the aerodynamic response time to the wall time. The wall velocity U_τ and the friction Reynolds number Re_τ are also defined.

$$t^+ = \frac{\nu \rho}{\tau_w}. \tag{19}$$

$$\tau_p^+ = \tau_p \Big/ t^+. \tag{20}$$

$$U_\tau = \sqrt{\frac{\tau_w}{\rho}}. \tag{21}$$

$$\mathrm{Re}_\tau = \frac{h U_\tau}{\nu}. \tag{22}$$

Within the channel the nondimensionalized gravitational constant G in wall units is given in equation 23. The Froude number Fr is the ratio of the inertial force to the gravitational force and can be computed by multiplying G by the Stokes number and taking the reciprocal, as shown in equation 24. The larger the Fr number the less important gravity is in the simulation. For this simulation $G = 3.6 \times 10^{-6}$ and Fr = 9. This indicates that for this simulation, gravity is not as important as the inertia, but probably not negligible. For the primer firings in open air (*24*) the particles seem to congregate predominately in the lower half of the explosion event. This would indicate that gravitational forces are important in the open-air firings.

$$G = \frac{g\nu}{U_\tau^3}. \tag{23}$$

$$Fr = \frac{U_\tau^3}{g\nu\tau_p^+}. \tag{24}$$

5.2 Definition of the Deposition Velocity V_d^+

To ensure proper mass balance across the flow channel requires a knowledge of the number of particles which enter the tube (based on the number of particles in the original primer mix) and the number of particles which hit the channel wall due to both gravitational effects and turbulent effects. In order to properly account for mass loss to the walls the so called deposition velocity, V_d, is introduced. It is not a velocity at all, but rather a deposition rate constant which has units of distance per time, the same units as a velocity. Because of this it was called a deposition velocity, but has nothing to do with the velocity of the particle at the time of impact. Some may confuse the deposition velocity with the wall normal velocity of a particle at impact, but there is no correlation whatsoever. The definition of the deposition velocity is

$$V_d = \frac{N}{c}, \tag{25}$$

where c is the mass of the particles per unit volume in the channel and N is the mass flux. All simulations done in this work are done with monodisperse particles so that

$$c = m_p n \tag{26}$$

and

$$N = m_p j, \tag{27}$$

where n is the number of particles per unit volume, j is the number flux of particles that deposit on the channel walls, and m_p is the mass of a single particle. It is useful to define the dimensionless deposition velocity in wall units. Combining these equations and making the result non-dimensional yields

$$V_d^+ = \frac{V_d}{U_\tau} = \frac{j}{nU_\tau}. \tag{28}$$

While investigating the deposition of particles on channel walls with small nondimensionalized radii (r/h), Schmidt et al. (*52*) demonstrated that the steady-state deposition velocity is independent of Reynolds numbers for Stokes numbers τ_p^+ from values of 10 to 25000. Above 25000 there is a slight Reynolds number dependence, with the highest Re having the greatest deposition.

For a first approximation a stibnite particle with a small r/h and a St τ_p^+ of 30000 was simulated in PODT at two different bulk Reynolds numbers around 12000 to compare to Schmidt et al. (*52*). Excellent agreement with Schmidt et al. was achieved, thereby verifying the use of this method to simulate the primer tube particles.

The simulation was repeated for a single Re with the radius of a representative stibnite particle actually used in the primer mix (r/h = 0.036). The larger diameter particle caused a higher deposition velocity. This is a phenomena not previously demonstrated in the literature.

6. Conclusions

Based on the experiments of Williams et al. (*24*), the corresponding Cheetah code gun calculations which assume stibnite and barium nitrate remain in the solid phase provides reasonable agreement. Verification of the PODT model in the range of interest to primer no. 41 simulations, with known deposition velocities, was achieved. A new diameter dependence on deposition velocity was noted. The PODT model has been assessed to be reasonably well suited to serve as an input to the NGEN code for small-caliber ammunition simulations. The PODT model predicted streamwise particle velocities inside the steady-state flow channel to be 47.5 m/s, where measurements just outside of the primer tube (*24*), in an open-air firing, yielded 45 m/s.

7. Future Work

The extension of PODT to large-caliber ignition systems is of interest. As can be seen in figure 1, the conventional ignition system for a large-caliber (120-mm) gun consists of a long, narrow metallic tube that is mounted on the cartridge case base (housing the igniter), which extends into the gun chamber along the chamber centerline and is sealed at the other end. Along its length, this primer tube is perforated with regularly spaced holes which allow radial and azimuthal venting of igniter gases. The tube contains an energetic material that generally consists of tightly-packed grains (smaller in diameter than the primer tube holes) designed to rapidly ignite and flamespread producing hot gases and hot solid particles. The efflux from the primer tube is used to ignite the solid propellant gun charge.

Primer models that include first-order effects (i.e., gas generation in a tabular form) have been used successfully to predict the performance of a number of large-caliber Army guns but are somewhat inconsistent with the multiphase Lagrangian approach used to model the solid propellant charge in the Army's NGEN code. It has long been considered a viable task to upgrade the treatment for the primer tube in a manner consistent with the NGEN code in a way

that explicitly treats the multiphase nature of the energetic material in the primer. Though the primer tube is essentially three-dimensional by its nature, an attempt has been made to develop a one-dimensional numerical model which will capture enough of the essential physics to predict semiquantitatively the burnout of these primer particles yet to be simple enough to be useful in providing the flow rates of gas and particles through the primer holes. The fate of the gas/particles from the primer efflux will then be determined using the NGEN IB model, i.e., the primer model would be in some fashion linked to the IB model.

Large-caliber ignition systems can be viewed as an array of particles in a turbulent channel which are allowed to leave the domain through a vent hole. PODT can be used to model this by adding many particles to the channel flow ODT code using one-way coupling to simulate a simple packed bed. Combustion of the particles would be simulated by igniting one end of the packed bed and allowing flame spreading down the bed. Particles would be allowed to heat up until the temperature was high enough to start combustion. The rate of combustion and combustion chemistry would be commensurate with current state-of-the-art IB modeling. Each representative particle would be tracked individually. A schematic of the piccolo tube primer model can be seen in figure 6. Each particle has an individual temperature, mass, velocity field, and position. As such, the particles can be ensemble averaged to produce look-up tables which may be used in NGEN or for simpler IB codes.

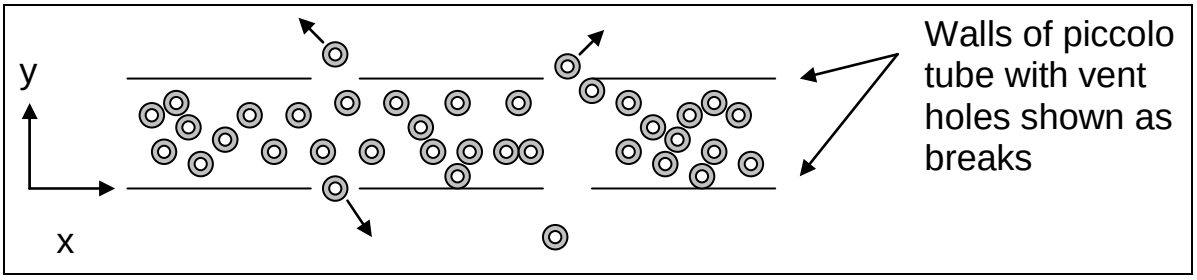

Figure 6. Large-caliber gun primer tube concept.

8. References

1. Anderson, R.; Fickie, K. *IBHGV2 – A User's Guide*; BRL-TR-2829; U.S. Army Ballistic Research Laboratory: Aberdeen Proving Ground, MD, July 1987.

2. Gough, P. S. *Interior Ballistics Modeling: Extensions to the XKTC Code and Analytical Studies of Pressure Gradient for Lumped Parameter Codes*; ARL-CR-460; U.S. Army Research Laboratory: Aberdeen Proving Ground, MD, February 2001.

3. Minor, T. C.; Horst, A. W. *Theoretical and Experimental Investigation of Flamespreading Processes in Combustible-Cased Stick Propelling Charges*; BRL-TR-2710; U.S. Army Ballistic Research Laboratory: Aberdeen Proving Ground, MD, February 1986.

4. Gough, P. S. Modeling Arbitrarily Packaged Multi-Increment Solid Propellant Charges of Various Propellant Configurations. *Proceedings of the 33rd JANNAF Combustion Meeting*, November 1996, CPIA publication no. 653, *1*, pp 421–435. (See also Gough, P. S. *Formulation of a Next-Generation Interior Ballistic Code*; ARL-CR-68; U.S. Army Research Laboratory: Aberdeen Proving Ground, MD, September 1993.)

5. Nusca, M. J.; Gough, P. S. *Numerical Model of Multiphase Flows Applied to Solid Propellant Combustion in Gun Systems*; AIAA Paper No. 98–3695, July 1998.

6. Nusca, M. J. *High-Performance Computing and Simulation for Advanced Armament Propulsion*; ARL-TR-3215; U.S. Army Research Laboratory: Aberdeen Proving Ground, MD, June 2004.

7. Horst, A. W.; Nusca, M. J. The Charge Designer's Workbench: A Range of Interior Ballistic Modeling Tools. *Proceedings of the 53rd JANNAF Propulsion Meeting*, Monterey, CA, 5–8 December 2005.

8. Gough, P. S. Modeling Chemical Interactions in Ignition of Gun Propellants. *Proceedings of the 22nd JANNAF Combustion Meeting*, October 1983, CPIA publication no. 432, *1*, Pasadena, CA.

9. Keller, G. E.; Horst, A. W. *The Two Phase Flow Simulation of LOVA Propellant Interior Ballistic Behavior Using the XNOVAK Code*; BRL-TR-2796; U.S. Army Ballistic Research Laboratory: Aberdeen Proving Ground, MD, April 1987.

10. Davis, T. L. *The Chemistry of Powder and Explosives*. John Wiley & Sons, Inc.: New York, NY, 1943.

11. Ekstedt, E. E.; Vest, D. C.; Emerson, V. C.; Dean, L. W. *Pressure Studies of Artillery Primers Fired Statically*; BRL report no. 938; U.S. Army Ballistic Research Laboratory: Aberdeen Proving Ground, MD, June 1955, p 9.

12. Chang, L.; Rocchio, J. J. *Simulator Diagnostics of the Early Phase Ignition Phenomena in a 105-mm Tank Gun Chamber*; BRL-TR-2890; U.S. Army Ballistic Research Laboratory: Aberdeen Proving Ground, MD, March 1988.

13. Keller, G. E.; Anderson, R. D.; Horst, A. W. *The Influence of Ignition Stimulus on the Interior Ballistic Performance of High-Performance Tank Gun Ammunition*; ARL-TR-292; U.S. Army Research Laboratory: Aberdeen Proving Ground, MD, October 1993.

14. Nusca, M. J. Application of the NGEN Code to Solid Propellant Charges of Various Propellant Configurations. *Proceedings of the 33rd JANNAF Combustion Meeting*, CPIA publication no. 653, November 1996, pp 421–435.

15. *Encyclopedia of Explosives and Related Items*; Vol. 8; Picatinny Arsenal: Dover, NJ, 1978.

16. Chamot, E. M. *The Microscopy of Small Arms Primers*. Cornell University Press: Ithaca, NY, 1922.

17. Ellern, H. *Modern Pyrotechnics, Fundamentals of Applied Physical Pyrochemistry*. Chemical Publishing Co., Inc.: New York, NY, 1961.

18. Kerstein, A. R.; Ashurst, W. T.; Nilsen, V.; Wunsch, S. E. One-Dimensional Turbulence: Vector Formulation and Application to Free Shear Flows. *J. Fluid Mech.* **2001**, *447*, 85–109.

19. Schmidt, J. R. Stochastic Models for the Prediction of Individual Particle Trajectories in One Dimensional Turbulence Flows. Ph.D. Dissertation, University of Arizona, Tucson, AZ, 2004.

20. Pope, S. B. *Turbulent Flows*. Cambridge University Press: New York, NY, 2000.

21. Young, J.; Leeming, A. A Theory of Particle Deposition in Turbulent Pipe Flow. *J. Fluid Mech.* **1997**, *340*, 129–159.

22. Call, C. J.; Kennedy, I. M. Droplet Dispersion, Velocity and Vaporization in Heated and Unheated Jets. *31st Aerospace Sciences Meeting and Exhibit, AIAA 93-0904*, Reno, NV, 1993.

23. Call, C. J.; Kennedy, I. M. Measurements of Droplet Dispersion in Heated and Unheated Turbulent Jets. *AIAA Journal* **1994**, *32*, 874–875.

24. Williams, A. W.; Brant, A. L.; Kaste, P. J.; Colburn, J. W. Experimental Studies of Primer Ignition in 5.56 Ammunition. *Proceedings of the 53rd JANNAF Propulsion Meeting*, 5–8 December 2005, Monterey, CA.

25. Kuo, K. K.; Moore, B. B.; Chen, D. Y. Characterization of Mass Flow Rates for Various Percussion Primers. *Gasdynamics of Detonations and Explosives*, Bowen, J. R., Manson, N., Oppenheim, A. K., Soloukhin, R. I., Eds.; AIAA Progress Series, *75*, pp 323–337, 1981.

26. Fried, L. E.; Glaesemann, K. R.; Howard, W. M.; Souers, P. C.; Vitello, P. A. Cheetah Code, Version 4.0, UCRL-CODE-155944, 2005.

27. Meyer, R.; Kohler, J.; Homburg, A. *Explosives*; 5th ed.; Wiley-VCH Publishing Co.: Germany, 2002.

28. Fox, W.; Vogelsang, K.; Harris, J.; Lathrop, A. Invesigation of Tetracene Decomposition Variation Using Taguchi Methodology. In *Military Mathematical Modeling (M3)*; Arney, D. C., Ed.; Department of Mathematical Sciences: United States Military Academy, West Point, NY, 1998.

29. McNesby, K. U.S. Army Research Laboratory. Personal communication, 11 November 2005.

30. Brauer, K. Handbook of Pyrotechnics; Chemical Publishing Co., Inc.: New York, 1974.

31. Bordon, S.; Campbell, C. *Differential Thermal Analysis of Inorganic Compounds, Nitrates and Perchlorates of the Alkali and Aldaline Earth Groups and Their Subgroups, Analytical Chemistry*; *27*, 1102–9, 1955.

32. Hinze, J. O. *Turbulence*. McGraw-Hill Book Company; 2nd ed.; 1975.

33. Stock, D. E. Particle Dispersion in Flowing Gases–1994 Freeman Scholar Lecture. *Transactions of the ASME* **1996**, *118*, 4–17.

34. Maxey, M. R.; Riley, J. J. Equation of Motion for a Small Rigid Sphere in Nonuniform Flow. *Phys. Fluids* **1983**, *26*, 883–888.

35. Wells, M. R.; Stock, D. E. The Effects of Crossing Trajectories on the Dispersion of Particles in a Turbulent Flow. *J. Fluid Mech*. **1983**, *136*, 31–62.

36. Sirignano, W. A. *Fluid Dynamics and Transport of Droplets and Sprays*. Cambridge University Press: United Kingdom, 1999.

37. Elghobashi, S. Particle-Laden Turbulent Flows: Direct Simulation and Closure Models. *Appl. Sci. Res*. **1991**, *48*, 301–314.

38. Elghobashi, S. On Predicting Particle-Laden Turbulent Flows. *Appl. Sci. Res*. **1994**, *52*, 309–329.

39. Zhang, H.; Ahmadi, G.; Fan, F.-G.; McLaughlin, J. B. Ellipsoidal Particles Transport and Deposition in Turbulent Channel Flows. *Int. J. Multiphase Flow* **2001**, *27*, pp 971–1009.

40. van Haarlem, B.; Boersma, B. J.; Nieuwstadt, F. T. M. Direct Numerical Simulation of Particle Deposition Onto a Free-Slip and No-Slip Surface. *Physics of Fluids* **1998**, *10*, 2608–2620.

41. Zhang, H.; Ahmadi, G. Aerosol Particle Removal and Re-Entrainment in Turbulent Channel Flows—A Direct Numerical Simulation Approach. *J. Adhesion* **2000**, *74*, 441–493.

42. Rouson, D. W.; Eaton, J. K. On the Preferential Concentration of Solid Particles in Turbulent Channel Flow. *J. Fluid Mech*. **2001**, *428*, 149–169.

43. Wang, Q.; Squires, K. D. Large Eddy Simulation of Particle-Laden Turbulent Channel Flow. *Int. J. Multiphase Flow* **1996**, *22*, 667–683.

44. Segura, J. C.; Eaton, J. K.; Oefelein, J. C. *Predictive Capabilities of Particle-Laden Large Eddy Simulation*; Mech. Engng. Dept. Rep. TSD-156; Stanford University: Stanford, CA, 2004.

45. McLaughlin, J. B. Aerosol Particle Deposition in Numerically Simulated Channel Flow. *Phys. Fluids* **1989**, *A 1*, 1211–1224.

46. Chen, M.; McLaughlin, J. B. A New Correlation for the Aerosol Deposition Rate in Vertical Ducts. *J. Colloid Interface Sci*. **1995**, *169*, 437–455.

47. Ounis, H.; Ahmadi, G.; McLaughlin, J. B. Dispersion and Deposition of Brownian Particles from Point Souces in Simulated Turbulent Channel Flow. *J. Colloid Interface Sci*. **1991**, *147*, 233–250.

48. Wang, Q.; Squires, K. D. Large Eddy Simulation of Particle Deposition in a Vertical Turbulent Channel Flow. *Int. J. Multiphase Flow* **1996**, *22*, 667–683.

49. Wang, Q.; Squires, K. D.; Chen, M.; McLaughlin, J. B. On the Role of the Lift Force in Turbulence Simulations of Particle Deposition. *Int. J. Multiphase Flow* **1996**, *23*, 749–763.

50. Schmidt, J. R. Trajectories of Evaporating Droplets in a Turbulent Combustor Using the One Dimensional Trubulence Model. Masters Thesis, University of Arizona, 2000.

51. Williams, A. W. U.S. Army Research Laboratory. Personal communication, November 2005.

52. Schmidt, J. R.; Went, J. O. L. W.; Kerstein, A. R. Effects of Inertia on Wall Deposition in Particle-Laden Turbulent Channel Flow. *Physics of Fluids*, submitted for publication, 2006.

INTENTIONALLY LEFT BLANK.

Appendix. Cheetah 4.0 Summary Sheet

```
##########################################################################
#                                                                        #
#                  CHEETAH 4.0 SUMMARY SHEET                             #
#                  Energetic Materials Center                            #
#              Lawrence Livermore National Laboratory                    #
#              Technical Contact: Dr. Laurence E. Fried                  #
#            Copyright 2004, Regents University of California            #
#                     All Rights Reserved                                #
#                                                                        #
##########################################################################
```

Product library title: the blake product library
Reactant library title: # Reactant library 4.0 by W.M. Howard. Fri Nov 25 15:01:13 EST 2005

The composition:

Name	% wt.	% mol	% vol	Heat of formation (cal/mol)	Mol. wt.	TMD (g/cc)	
petn	9.43	4.97	14.23	-127151	316.13	1.78	n 4 c 5 h 8 o 12
tetrazene	7.55	6.68	11.91	45172	188.15	1.70	c 2 n 10 o 1 h 8
al	9.25	57.07	9.19	0	26.98		2.70 al 1
al2o3	3.96	6.47	2.66	-399092	101.96	3.99	o 3 al 2
lead styph	69.81	24.82	62.01	-260277	468.30	3.02	o 9 n 3 pb 1 c 6 h 3

library file, blake.chl
composition, petn, 9.43, tetrazene, 7.55, al, 9.25, al2o3, 3.96, lead styph, 69.81, weight
gun, 0.0139, 0.05, 0.0139

CHEETAH version 4.0
Energetic Materials Center
Lawrence Livermore National Laboratory
Technical contact: Dr. Laurence E. Fried

The time is Wed Jan 18 14:35:10 2006

Version Tag: 280
Code build date: 18 Jan 2005
Code date = 2005/01/15 00:10:57

This appendix appears in its original form, without editorial change.

Library Title: the blake product library
Executing library command: gas eos, virial
Input>library file, blakejrs.chl
Product library title: the blake product library
Executing library command: gas eos, virial
Input>composition, petn, 9.43, tetrazene, 7.55, al, 9.25, al2o3, 3.96, lead styph, 69.81, weight
Reactant library title:# Reactant library 4.0 by W.M. Howard. Fri Nov 25 15:01:13 EST 2005

The Composition

Name	% wt.	% mol	%vol.	Heat of Formation (cal/mol)	Standard volume (cc/mol)	Standard entropy (cal/K/mol)	Mol. wt.	Formula
Petn	9.43	4.97	14.23	-127151	177.80	0.000	316.13	n4c5h8o12
Tetrazene	7.55	6.68	11.91	45172	110.68	0.000	188.15	c2n10o1h8
al	9.25	57.07	9.19	0	9.99	0.000	26.98	al1
al2o3	3.96	6.47	2.66	-399092	25.55	0.000	101.96	o3al2
lead styph	69.81	24.82	62.01	-260277	155.07	0.000	468.30	o9n3pb1c6h3

Heat of formation = -562.799 cal/gm
Standard volume = 0.373 cc/gm
Standard entropy = 0.000 cal/k/gm
Standard energy = -562.808 cal/gm

The elements and percent by mole

n	17.519
c	20.343
h	18.226
o	33.601
al	7.612
pb	2.698

The average mol. wt. = 166.476 g/mol
Input>gun, 0.0139, 0.05, 0.0139
GUN calculation:

	Rho g/cc	Temp K	Pressure MPa	Impetus J/g	Mol Wt. Gas	Covol cc/g	Frozen Cp/Cv	Phi
1.)	0.0139	2797.1	7.4	526.75	44.153	0.635	1.176	1.009

Product concentrations

Name	Phase	(mol/kg)	(mol gas/mol explosive)
co	Gas	1.096e+001	1.825e+000
n2	Gas	4.838e+000	8.054e-001
h2	Gas	4.252e+000	7.079e-001
pb	Gas	1.482e+000	2.466e-001
h2o	Gas	7.313e-001	1.217e-001
co2	Gas	2.726e-001	4.539e-002
h	Gas	9.275e-002	1.544e-002
opb	Gas	9.166e-003	1.526e-003
oh	Gas	4.559e-003	7.589e-004
hcn	Gas	1.634e-003	2.720e-004
nh3	Gas	5.180e-004	8.624e-005

no	Gas	4.265e-004	7.101e-005
cho	Gas	3.140e-004	5.227e-005
alho2	Gas	2.544e-004	4.235e-005
ch2o	Gas	8.735e-005	1.454e-005
o	Gas	6.164e-005	1.026e-005
hnco	Gas	4.291e-005	7.143e-006
al	Gas	4.170e-005	6.943e-006
nh2	Gas	3.852e-005	6.412e-006
ch4	Gas	1.204e-005	2.004e-006
al2o	Gas	9.490e-006	1.580e-006
formac	Gas	9.379e-006	1.561e-006
ch3	Gas	6.115e-006	1.018e-006
nh	Gas	4.697e-006	7.819e-007
o2	Gas	4.237e-006	7.053e-007
n	Gas	4.196e-006	6.985e-007
cn	Gas	3.702e-006	6.163e-007
c2h2	Gas	1.092e-006	1.818e-007
hno	Gas	7.174e-007	1.194e-007
nco	Gas	4.343e-007	7.230e-008
ch2	Gas	2.759e-007	4.593e-008
ketene	Gas	2.201e-007	3.664e-008
n2o	Gas	9.607e-008	1.599e-008
halo	Gas	8.573e-008	1.427e-008
alo2	Gas	4.223e-008	7.029e-009
h2o2	Gas	3.165e-008	5.269e-009
ho2	Gas	3.137e-008	5.223e-009
ch2oh	Gas	2.178e-008	3.626e-009
ch4o	Gas	2.112e-008	3.517e-009
c	Gas	5.157e-009	8.586e-010
c2h4	Gas	3.822e-009	6.363e-010
no2	Gas	2.088e-009	3.476e-010
hno2	Gas	1.137e-009	1.892e-010
ch3cn	Gas	9.338e-010	1.555e-010
al2o3	liquid	2.102e+000	3.500e-001
*pb	liquid	0.000e+000	0.000e+000
*pb	solid	0.000e+000	0.000e+000
c(s)	solid	0.000e+000	0.000e+000
al2o3	solid	0.000e+000	0.000e+000
Total Gas	2.265e+001	3.770e+000	
Total Cond.	2.102e+000	3.500e-001	

NO. OF
COPIES ORGANIZATION

1 (PDF ONLY) DEFENSE TECHNICAL INFORMATION CTR
DTIC OCA
8725 JOHN J KINGMAN RD
STE 0944
FORT BELVOIR VA 22060-6218

1 US ARMY RSRCH DEV & ENGRG CMD
SYSTEMS OF SYSTEMS INTEGRATION
AMSRD SS T
6000 6TH ST STE 100
FORT BELVOIR VA 22060-5608

1 INST FOR ADVNCD TCHNLGY
THE UNIV OF TEXAS
AT AUSTIN
3925 W BRAKER LN
AUSTIN TX 78759-5316

1 DIRECTOR
US ARMY RESEARCH LAB
IMNE ALC IMS
2800 POWDER MILL RD
ADELPHI MD 20783-1197

3 DIRECTOR
US ARMY RESEARCH LAB
AMSRD ARL CI OK TL
2800 POWDER MILL RD
ADELPHI MD 20783-1197

ABERDEEN PROVING GROUND

1 DIR USARL
AMSRD ARL CI OK TP (BLDG 4600)

NO. OF COPIES ORGANIZATION

1 DIRECTOR
US ARMY RESEARCH LAB
AMSRD ARL D
J MILLER
2800 POWDER MILL RD
ADELPHI MD 20783-1197

3 DIR USARL
AMSRD ARL RO P
D MANN
R SHAW
TECH LIB
PO BOX 12211
RESEARCH TRIANGLE PARK NC
27709-2211

8 US ARMY AVIATN & MSLE CMD
AMSRD AMR PS PT
W CHEW
C DOLBEER
J S LILLY
M LYON
J M FISHER
B P MARSH
R S MICHAELS
D THOMPSON
REDSTONE ARSENAL AL 35898-5249

2 PM MAS
SFAE AMO MAS
LTC M BUTLER
PICATINNY ARSENAL NJ 07806-5000

2 PM CAS
SFAE AMO CAS
PICATINNY ARSEBAL NJ 07806-5000

1 US ARMY ARDEC
AMSRD AAR EMB
R CARR
BLDG 1
PICATINNY ARSENAL NJ 07806-5000

1 US ARMY ARDEC
SFAE AMD CAS
R CIRINCIONE
BLDG 171
PICATINNY ARSENAL NJ 07806-5000

1 US ARMY ARDEC
AMSRD AAR AEE W
S EINSTEIN
BLDG 382
PICATINNY ARSENAL NJ 07806-5000

NO. OF COPIES ORGANIZATION

1 US ARMY ARDEC
AMSRD AAR AEE W
P HUI
BLDG 382
PICATINNY ARSENAL NJ 07806-5000

1 US ARMY ARDEC
AMSRD AAR D
J LANNON
BLDG 1
PICATINNY ARSENAL NJ 07806-5000

1 US ARMY ARDEC
B MACHAK
AMSRD AAR ATD
BLDG 1
PICATINNY ARSENAL NJ 07806-5000

1 US ARMY ARDEC
AMSRD AAR AEE W
S NICOLICH
BLDG 3022
PICATINNY ARSENAL NJ 07806-5000

1 US ARMY ARDEC
P O REILLY
BLDG 3022
PICATINNY ARSENAL NJ 07806-5000

1 US ARMY ARDEC
J O REILLY
BLDG 382
J RUTKOWSKI BLDG 171M
PICATINNY ARSENAL NJ 07806-5000

1 US ARMY ARDEC
A SABASTO
BLDG 94
PICATINNY ARSENAL NJ 07806-5000

1 US ARMY ARDEC
AMSRD AAR AEE W
J SHIN
BLDG 382
PICATINNY ARSENAL NJ 07806-5000

1 US ARMY ARDEC
AMSRD AAR AEE W
R SURAPANENI
BLDG 3022
PICATINNY ARSENAL NJ 07806-5000

NO. OF COPIES ORGANIZATION

1 COMMANDER
RADFORD ARMY AMMO PLANT
SMCAR QA HI LIB
RADFORD VA 24141-0298

1 RAYTHEON MISSILE SYSTEMS
D BLANCHARD
8634 E OLINGA CT
TUCSON AZ 85747

8 DIR BENET WEAPONS LAB
M AUDINO
R DILLON
R FISCELLA
R HASENBEIN
E KATHE
K MINER
S SOPOK
J MCNEIL
WATERVLIET NY 12189-4000

1 COMMANDANT
USAFC&S
ATSF CN P GROSS
FT SILL OK 73503-5600

2 CDR NAVAL RSRCH LAB
TECH LIBRARY
J BORIS
WASHINGTON DC 20375-5000

1 OFFICE OF NAVAL RSRCH
J GOLDWASSER
875 N RANDOLPH ST RM 653
ARLINGTON VA 22203-1927

6 CDR
NAVAL SURFACE WARFARE CTR
R DOHERTY R2A
C GOTZMER TM3
C MICHIENZI R22
S MITCHELL OPA
S C SMITH R3A
TECHLIB
INDIAN HEAD MD 20640-5000

5 CDR
NAVAL SURFACE WARFARE CTR
J FRAYSEE G33
R FRANCIS T08
T C SMITH
T TSCHIRN G30
TECHLIB
DAHLGREN VA 22448-5000

NO. OF COPIES ORGANIZATION

3 CDR
NAVAL AIR WARFARE CTR
A ATWOOD
S BLASHILL
T PARR
CHINA LAKE CA 93555-6001

1 AIR FORCE RESH LAB
MNME EN MAT BR
B WILSON
2306 PERIMETER RD
EGLIN AFB FL 32542-5910

1 AIR FORCE OFC OF SCI RSRCH
M BERMAN
875 N RANDOLPH ST
STE 235 RM 3112
ARLINGTON VA 22203-1768

1 NASA LANGLEY RSRCH CTR
D BUSHNELL
MAIL STOP 110
HAMPTON VA 23681-2199

1 DIR SANDIA NATL LABS
M BAER DEPT 1512
PO BOX 5800
ALBUQUERQUE NM 87185

2 DIR LAWRENCE LIVERMORE NL
L FRIED
M MURPHY
PO BOX 808
LIVERMORE CA 94550-0622

1 CENTRAL INTELLIGENCE AGNCY
J BACKOFEN
RM 4PO7 NHB
WASHINGTON DC 20505

1 BATTELLE EAST SCI & TECH
A ELLIS
1204 TECHNOLOGY DR
ABERDEEN MD 21001-1228

2 JHU CHEM PROP INFO AGNCY
W HUFFERD
R FRY
10630 LITTLE PATUXENT PKWY
STE 202
COLUMBIA MD 21044-3200

NO. OF COPIES ORGANIZATION

1 OUSD (AT&L)/STRAT & TACT SYS MUNITIONS
T MELITA
3090 DEFENSE PENTAGON
RM 3B1060
WASHINGTON DC 20301-3090

1 BRIGHAM YOUNG UNIV
DEPT OF CHEMICAL ENGRG
M BECKSTEAD
PROVO UT 84601

1 CALIF INSTITUTE OF TECHLGY
F E C CULICK
204 KARMAN LAB
MS 301 46
1201 E CALIFORNIA ST
PASADENA CA 91109

2 UNIV OF ILLINOIS
DEPT OF MECH INDUSTRY ENGRG
H KRIER
R BEDDINI
144 MEB 1206 N GREEN ST
URBANA IL 61801-2978

5 PENNSYLVANIA STATE UNIV
DEPT OF MECHANICAL ENGRG
K KUO
T LITZINGER
G SETTLES
S THYNELL
V YANG
UNIVERSITY PARK PA 16802-7501

1 ARROW TECHLGY ASSOC INC
1233 SHELBURNE RD D 8
SOUTH BURLINGTON VT 05403

1 ALLEGHENY BALLISTICS LAB
PO BOX 210
ROCKET CENTER WV 26726

1 ATK ORDNANCE
4700 NATHAN LANE
PLYMOUTH MN 55442

3 ATK AMMO & ENERGETICS
D A WORRELL
W J WORRELL
S RITCHIE
RADFORD ARMY AMMO PLANT
RT 114 PO BOX 1
RADFORD VA 24141-0299

NO. OF COPIES ORGANIZATION

4 ATK THIOKOL
P BRAITHWAITE
T B FARABAUGH
W B WALKUP
R WARDLE
PO BOX 707
BRIGHAM CITY UT 84302-0707

1 ATK ELKTON
J HARTWELL
PO BOX 241
ELKTON MD 21921-0241

1 BAE ARMAMENT SYS DIV
JAHN DYVIK
4800 EAST RIVER RD
MINNEAPOLIS MN 55421-1498

2 GEN DYNAMICS ORD/TACT SYS
N HYLTON
J BUZZETT
10101 DR M L KING ST N
ST PETERSBURG FL 33716

3 GENERAL DYNAMICS ST MARKS
J DRUMMOND
H RAINES
D W WORTHINGTON
PO BOX 222
SAINT MARKS FL 32355-0222

1 GENERAL DYNAMICS ARM SYS
J TALLEY
128 LAKESIDE AVE
BURLINGTON VT 05401

1 HICKS AND ASSOCIATES SAIC
I MAY
7990 SCIENCE APPLIC CT
VIENNA VA 22182

1 PAUL GOUGH ASSOC INC
P S GOUGH
1048 SOUTH ST
PORTSMOUTH NH 03801-5423

3 VERITAY TECHGY INC
R SALIZONI
J BARNES
E FISHER
4845 MILLERSPORT HWY
EAST AMHERST NY 14501-0305

NO. OF
COPIES ORGANIZATION

1 SRI INTERNATIONAL
PROPULSION SCIENCES DIV
TECH LIB
333 RAVENWOOD AVE
MENLO PARK CA 94025-3493

1 SAIC
M PALMER
1410 SPRING HILL RD
STE 400
MCLEAN VA 22102

1 NETWORK COMPUTING SERVICES
S RAY
1200 WASHINGTON AVE S
MINNEAPOLIS MN 55415

1 SANDIA NATIONAL LABS
A KERSTEIN
PO BOX 969 MS 9051
LIVERMORE CA 94551-0969

ABERDEEN PROVING GROUND

1 CDR USAATC
CSTE DTC AT SL
APG MD 21005

66 DIR USARL
AMSRD ARL WM B
C CANDLAND
J B MORRIS
J NEWILL
M ZOLTOSKI
AMSRD ARL WM BA
G BROWN
B DAVIS
D HEPNER
G KATULKA
T KOGLER
D LYON
AMSRD ARL WM BC
M BUNDY
G COOPER
J DESPIRITO
J GARNER
P PLOSTINS
J SAHU
S SILTON
P WEINACHT
AMSRD ARL WM BD
W R ANDERSON
R A BEYER

NO. OF
COPIES ORGANIZATION

A L BRANT
S W BUNTE
L M CHANG
T P COFFEE
J COLBURN
P J CONROY
N ELDREDGE
B E FORCH
B E HOMAN
AW HORST
S L HOWARD
P J KASTE
A J KOTLAR
C LEVERITT
R LIEB
K L MCNESBY
M MCQUAID
A W MIZIOLEK
J E NEWBERRY
M J NUSCA (6 CPS)
R A PESCE-RODRIGUEZ
S PIRAINO
G P REEVES
B M RICE
R C SAUSA
J SCHMIDT (6 CPS)
A W WILLIAMS
AMSRD ARL WM BF
R D ANDERSON
W OBERLE
D WILKERSON
AMSRD ARL WM EG
E SCHMIDT
AMSRD ARL WM M
S MCKNIGHT
AMSRD ARL WM SG
W CIEPIELA
T ROSENBERGER
AMSRD ARL WM T
B BURNS
AMSRD ARL WM TB
P BAKER